Featuring work from the group of Samuel Sánchez at the Leibniz Institute for Solid State and Materials Research Dresden and the Max Planck Institute for Intelligent Systems Stuttgart, Germany.

Title: Thermal activation of catalytic microjets in blood samples using microfluidic chips

Self-propelled micromotors swim in microfluidic chips containing diluted blood samples at physiological temperature. Motors can be remotely guided by small magnets to travel from one reservoir to another in an accurate manner.

As featured in:

Lab on a Chip

See Lluís Soler, Samuel Sánchez *et al. Lab Chip*, 2013, 13, 4299.

Thermal activation of catalytic microjets in blood samples using microfluidic chips†

Lluís Soler,*[ab] Cynthia Martínez-Cisneros,[a] Anka Swiersy,[a] Samuel Sánchez*[ab] and Oliver G. Schmidt[ac]

We demonstrate that catalytic microjet engines can out-swim high complex media composed of red blood cells and serum. Despite the challenge presented by the high viscosity of the solution at room temperature, the catalytic microjets can be activated at physiological temperature and, consequently, self-propel in diluted solutions of blood samples. We prove that these microjets self-propel in 10× diluted blood samples using microfluidic chips.

The vision that tiny motors could one day navigate along bloodstreams still remains unrevealed. The emerging field of nanomotors is yet continuously reporting many exciting developments towards that and other bio-related directions.[1–5] Nowadays, there is a variety of artificial microswimmers that are, among others, electrochemically,[6,7] magnetically[8–12] or catalytically[13–19] powered. Catalytic micro- and nanomotors are self-propelled in chemical-rich fluids where they swim since they contain specially designed catalytic areas where hydrogen peroxide decomposes into molecular oxygen and water, leading to self-motile forces by different propulsive mechanisms.[1,17,20]

Amid the different mechanisms, bubble propulsion[19,21] has demonstrated potential applications from biosensing,[22–24] remediation,[25] and microsurgery[26,27] to selective cell transport.[5,23] In addition, this mechanism enables the self-propulsion of microjets in ionic media and complex environments such as (highly diluted) serum, urine and saliva,[23,28] making the bubble-propelled microjets more versatile than nanorod motors based on the electrokinetic mechanism. Wang's group presented interesting and novel lab-on-a-chip concepts based on the active motion of artificial microjets integrating several steps of an analytical process, including capture, transport, tagging and detection of biomaterials.[29,30] If biological samples are to be analysed, however, one of the remaining tasks is hence to demonstrate biocompatibility of the fuel and the viability of the bioorganisms at those conditions where the micromotors swim and actuate. We previously reported that at low concentrations of hydrogen peroxide (0.2 wt.%), and at physiological temperatures, the microjets are capable of swimming in a suspension of fibroblast cells for a short period, *ca.* 30 min, before most of the cells undergo apoptosis.[31] This issue could also be seen as a motivation to find different conditions (*e.g.* physiological temperatures) where the micromotors could still develop some advanced tasks as suggested in the literature.

In a previous issue of this journal, Pumera and co-workers reported some of the challenges for the self-propulsion of microjets in blood.[32] The authors showed that neither rolled-up microjets nor electrochemically produced microjets could overcome Brownian motion in blood solutions at room temperature. They also reported that for the microjets to move, the blood needs to be at least 100× diluted.

Here, we demonstrate that rolled-up microjets can indeed self-propel in 10× diluted samples at 37 °C, *i.e.* physiological temperatures (see schematic representation in Fig. 1). We performed temperature cycles of five minutes at 25 and 37 °C, respectively, proving that catalytic microjets are able to self-propel in highly complex media. In this approach, the viscosity of the solution is decreased and the activity of micromotors is enhanced by increasing the temperature of the solution. This work is by no means claiming that the current state of research in self-propelled micromotors enables their motion in bloodstreams. We aim here to prove that the high viscosity of blood at room temperature will not allow the motion of catalytic microjets, but the propulsion in warmer solutions of diluted blood samples is still possible. This discovery might be important for biosensing applications on-chip.

[a] Institute for Integrative Nanosciences, Leibniz Institute for Solid State and Materials Research Dresden, Helmholtzstraße 20, 01069 Dresden, Germany. E-mail: soler@is.mpg.de, sanchez@is.mpg.de; Tel: +49 711 689 1846
[b] Max Planck Institute for Intelligent Systems, Heisenbergstr. 3, D-70569 Stuttgart, Germany
[c] Materials Systems for Nanoelectronics, TU Chemnitz, 09107 Chemnitz, Germany
† Electronic supplementary information (ESI) available: Supporting videos, Fig. S1 and experimental section. See DOI: 10.1039/c3lc50756d
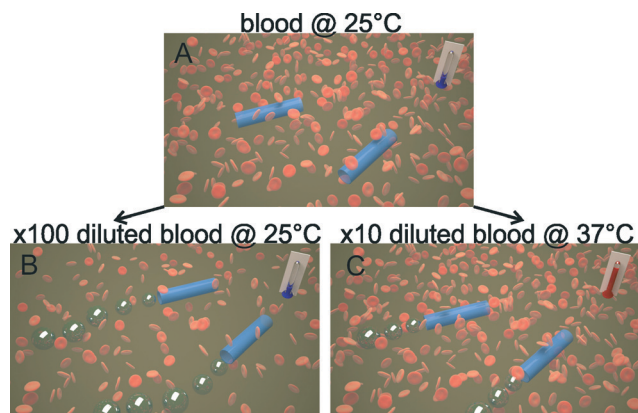
Fig. 1 Schematic representation of the behaviour of microjet engines in reconstituted blood samples. A) Inactive tubes at 25 °C at real blood concentration. B) Microjets self-propel at 25 °C when blood samples are 100× diluted. C) Microjets can also self-propel if 10× diluted blood is kept at a physiological temperature of 37 °C.

Furthermore, we fabricated a microfluidic chip containing solutions of 10× diluted blood and controlled the temperature at 37 °C, where catalytic microjets can self-propel along with red blood cells (RBC). This work may support the microtransporter-based lab-on-a-chip concept for *in vitro* sensing of diluted real samples.[29,30]

Microjets were fabricated by rolled-up nanotechnology on polymers as reported elsewhere in detail and in the ESI ([1,33]). In this work, we prepared rolled-up microtubes consisting of Fe/Pt nanomembranes (6/1 nm) deposited onto photoresist squared patterns of 50 μm^2.

Studies of motion of microjets in several samples of blood components were performed in a phosphate-buffered saline (PBS) solution containing the microjets and constant concentrations of surfactant and hydrogen peroxide (1 wt.% sodium dodecyl sulphate (SDS), 3 wt.% H_2O_2) in a total volume of 1 mL. These conditions will be used in the entire manuscript for all experiments. Red blood cells were reconstituted in 10 ml PBS to achieve an ~10% hematocrit. Before each experiment with RBC, their concentration was quantified in a counting chamber with 10 μL of a 1000× diluted reconstituted RBC sample. After that, the required amount of the reconstituted RBC sample was pipetted to prepare a 1 mL suspension of RBC at a concentration of 5×10^5 RBC μL^{-1}, which corresponds to a 10 times dilution compared to the typical concentration of RBC in blood (5×10^6 RBC μL^{-1}). To evaluate the micromotor performance on a chip, a polydimethylsiloxane (PDMS)-based microfluidic device was fabricated using soft lithography. The PDMS pre-polymer (10:1 w/w) (SYLGARD 184, Dow Corning GmbH, Germany) was cast onto a COC (cyclic olefin copolymer) master with a thickness of 1 mm and cured at 80 °C for 1 hour. Once cured, the microstructured PDMS replica was carefully peeled off from the master and bonded to a glass substrate. To enhance the bonding process and activate the PDMS surface to make it hydrophilic, both materials were treated with oxygen plasma at 30 W for 30 s. The final dimensions of the channel were 1 mm wide, 20 mm long and 1 mm deep.

As a control experiment, we first evaluated the speed variation of the catalytic microjets at room temperature (25 °C) and at physiological temperature (37 °C) in 1 mL PBS solution containing 3 wt.% H_2O_2 and 1 wt.% SDS, performing temperature cycles of 5 minutes between 25 and 37 °C. As previously demonstrated,[31] the microjets accelerate by increasing the temperature of the fuel solution and can react to temperature cycles. We observed a drift to higher velocities with the number of cycles, which may indicate that the catalytic microjets become more active upon the temperature cycles. Velocities during the first cycle increase from 100 μm s^{-1} at 25 °C to 400 μm s^{-1} at 37 °C, whereas the speed at the third cycle varies from 280 to 800 μm s^{-1}, respectively (Fig. 2A). Optical microscopy images from microjets swimming at 25 and 37 °C are illustrated in Fig. 2B. The length of the bubble tail is related to the speed of microjets, since those propelled at 37 °C generate more bubbles per second than those propelled at 25 °C.

Afterwards, we immersed the micromotors in diluted suspensions of RBC, performing the same temperature cycles of 5 minutes between 25 and 37 °C. Fig. 2C shows the motion of microjets in a 1 mL suspension of RBC 10× diluted (5×10^5 RBC μL^{-1}). We observed that microjets did not move at all at 25 °C but they were "activated" upon increasing the temperature of the RBC suspension, reaching speeds of about 60 μm s^{-1} in the second cycle. The average speed at 37 °C over the four cycles was about 47 μm s^{-1}.

Since many factors may influence the dynamics of microjets, such as slight asymmetries in the geometry, dynamic flows in the solution, *etc.*, different microjets may result in variable absolute values of the speed. The tracked trajectories for the four cycles of representative microjets during 4 s are depicted in Fig. 2D. Black crosses at 25 °C for the first and second cycles indicate that no motion was observed. After increasing the RBC concentration up to a 5× dilution, we also observe motion of micromotors at 37 °C. However,
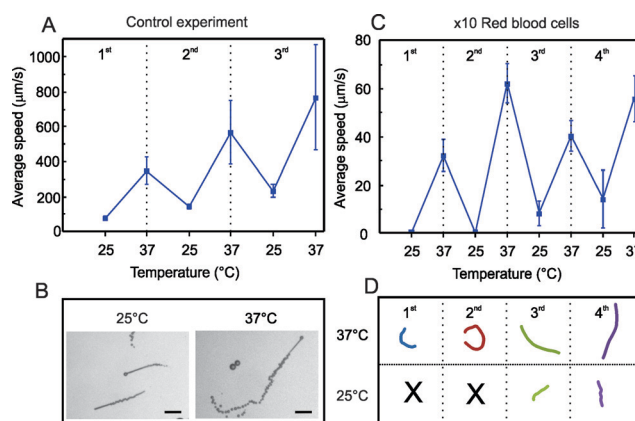
Fig. 2 Temperature cycles for activation of microjets. A) Motion of microjets in PBS solution. B) Snapshots of microjets and bubble tails at 25 and 37 °C, respectively. Scale bar: 50 μm. C) Motion of microjets in suspensions of red blood cells 10× diluted: average speeds during 4 temperature cycles of 5 min each between 25 and 37 °C. D) Tracked trajectories (4 s) for the 4 cycles of representative microjets.

the hostile experimental conditions such as the high viscosity and the high convection induced by the large amount of bubbles generated both by the microjets and the RBC complicate the quantitative evaluation of the speed. Indeed, higher dilutions of RBC lead to higher swimming velocities, as expected and as already reported by Pumera *et al.*[32] Nevertheless, the authors only reported quantitative speeds at dilutions up to 1000× RBC. Most strikingly, the authors did not consider experiments where the blood samples are maintained at physiological temperature, which makes a difference in terms of viscosity. Here, we report that the viscosity of the sample can be significantly reduced upon increasing the temperature of the solution to physiological levels, facilitating the self-propulsion of the microjets. The slight increase in the average speed with the temperature cycles (Fig. 2C), as occurred for microjets in PBS (Fig. 2A), and the motion at 25 °C after the second cycle, confirms that an activation of the microjets with the cycles is taking place. Therefore, we have a synergic effect between activating the catalytic propulsion of microjets and the reduction of the viscosity of the solutions.

A similar effect was observed when catalytic microjets were immersed in highly concentrated serum media, *i.e.* from 50 wt.% using the same fuel conditions (Fig. S1, A). Microjets immersed in 50% serum described slow motion already at 25 °C, and they accelerated at 37 °C. The viscosity of the solution varies from 1.2 at 25 °C to 1.0 at 37 °C. The microjets reach speeds up to 30 μm s^{-1} in 50 wt.% serum at 37 °C.

Microjets do not propel after 3 activation cycles in 80 wt.% serum solutions. We hypothesize that there might be other components from the complexity of the serum interfering with the catalytic area of the microjet engines. Samples containing serum at 90 wt.% led to the release of bubbles from microjets, but the high viscosity of the media impeded the forward motion.

Furthermore, we combined RBC 10× diluted with a solution of serum at 10 wt.% and applied three temperature cycles, as illustrated in Fig. 3. These conditions may correspond to a 10 times dilution of a real blood sample, resulting in a final concentration of 5×10^5 RBC μL^{-1}. Similar to Fig. 2, the microjets were not able to move significantly at 25 °C. In addition, due to the increase of viscosity after the addition of RBC in serum media, the absolute average speed at all temperatures decreased, reaching values from 15 to 25 μm s^{-1}. To demonstrate the effect of viscosity on the activation of the microjets, we monitored this parameter during the temperature cycles. As expected, and observed from Fig. 3A, viscosity is decreased when physiological temperatures are applied (37 °C), going to its initial value once room temperature is recovered.

According to these results, a trend relating viscosity and motion can be established. When the viscosity of the solution is higher than 1.1 mPa s, microjets cannot self-propel. Moreover, we found in this case a slight decrease in the mean velocity of the microjets with the temperature cycles. This might indicate that there are, besides the viscosity of the blood samples, other components from the serum that may
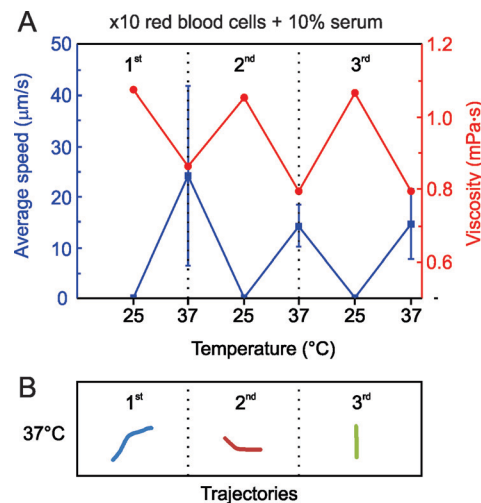

Fig. 3 Blood 10× diluted in 10 wt.% serum. A) Average speed of Fe/Pt microjets warming up the solution from 25 °C to 37 °C in three consecutive thermal cycles. B) Tracked trajectories (4 s) for the 3 cycles at 37 °C of representative microjets.

passivate with the experiment time and interfere with the motion of self-propelled microjets

Recently, the poisoning of self-propelled microjets by extracellular thiols was reported.[34] A more careful study regarding the effect of different components of blood on the motility of microjets should be addressed in the near future. Tracked trajectories at 37 °C for 4 s are shown in Fig. 3B.

Finally, we evaluated the microjets' performance in a microfluidic chip testing the same conditions for RBC 10× diluted in a 10 wt.% serum media (Fig. 4). We control the temperature of the microfluidic chip by placing it onto small Peltier elements as in previous experiments (Fig. 2 and 3). Using the microfluidic approach, it is possible to reduce the
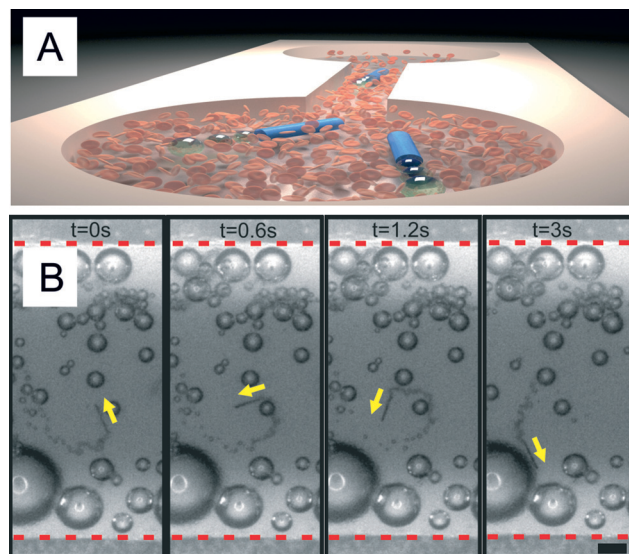
Fig. 4 Microjets moving together with diluted blood in microfluidic chips. A) Sketch of the motion of microjets moving from one side to the other of the microchip. B) Optical microscope images of a microjet engine moving against the flow in a microfluidic channel with blood 10× diluted at 37 °C. Scale bar: 50 μm.

consumption of reagents (*i.e.* blood sample) which is beneficial for scarce and highly valuable samples. The upper panel of Fig. 4 shows an illustration of the microfluidic setup utilized in this work (microjets and microchip not to scale). The lower panel shows a three-second motion sequence of a microjet moving in the microfluidic channel when the temperature was kept at 37 °C. The high viscosity and the presence of RBC did not prevent the microjets from moving from one reservoir to the other. We observed the continuous motion of microjets in the microfluidic chip over periods of 5 minutes. After this time, the appropriate visualization was impeded by the large amount of generated bubbles which accumulate at the top of the chip. This experiment demonstrates the proof-of-principle that microjets could be eventually employed for the active motion in lab-on-a-chip devices for, *e.g.*, biosensing, isolation of components, separation of different particles on a chip, *etc.* Microjets can self-propel into one reservoir placed at one side of the chip and swim to the other side along with the blood sample.

In order to fully confirm the viability of the active biosensing with catalytic microjets proposed in the literature, further research should address the transport of biomolecules or cells within microfluidic chips containing blood samples. Moreover, major efforts should be unleashed to find biocompatible fuels that propel microjets.

Conclusions

We demonstrated the activation of self-propelled microjets in blood samples at physiological temperatures. Microjets immersed in blood samples are unable to propel at 25 °C due to the high viscosity of the blood at those conditions. However, the synergic effect of reducing the viscosity upon increasing the temperature and the energetic activation of the catalytic microjets facilitates their movement in these complex media. We demonstrated that microjets are also able to move in highly concentrated serum samples, from 50% to 80%. We proved that microjets can actively propel in blood samples at a 10× dilution in batch and in a microfluidic device. Quantitative analysis on their motion indicates that with time, the microjets slow down in complex samples of blood 10× diluted. This indicates that other components of the blood samples may also interfere in the motility of catalytic microjets poisoning their catalytic surfaces. This effect should be the subject of further studies in the near future to understand the motility of micro-nanojets in real samples. This is one step towards their use in active biosensing devices and systems. Yet, it is still necessary to study issues like the viability of the components of blood (and not only RBC) in the fuel employed for the motion.

Acknowledgements

Notes and references

1 Y. F. Mei, A. A. Solovev, S. Sanchez and O. G. Schmidt, *Chem. Soc. Rev.*, 2011, **40**, 2109–2119.
2 J. Wang and W. Gao, *ACS Nano*, 2012, **6**, 5745–5751.
3 S. Sengupta, M. E. Ibele and A. Sen, *Angew. Chem., Int. Ed.*, 2012, **51**, 8434–8445.
4 D. Patra, S. Sengupta, W. T. Duan, H. Zhang, R. Pavlick and A. Sen, *Nanoscale*, 2013, **5**, 1273–1283.
5 S. Sanchez, A. A. Solovev, S. Schulze and O. G. Schmidt, *Chem. Commun.*, 2011, **47**, 698–700.
6 M. Sentic, G. Loget, D. Manojlovic, A. Kuhn and N. Sojic, *Angew. Chem., Int. Ed.*, 2012, **51**, 11284–11288.
7 G. Loget and A. Kuhn, *Lab Chip*, 2012, **12**, 1967–1971.
8 K. E. Peyer, L. Zhang and B. J. Nelson, *Nanoscale*, 2013, **5**, 1259–1272.
9 L. Zhang, T. Petit, K. E. Peyer and B. J. Nelson, *Nanomed.: Nanotechnol., Biol. Med.*, 2012, **8**, 1074–1080.
10 S. Tottori, L. Zhang, F. Qiu, K. K. Krawczyk, A. Franco-Obregón and B. J. Nelson, *Adv. Mater.*, 2012, **24**, 811–816.
11 A. Ghosh and P. Fischer, *Nano Lett.*, 2009, **9**, 2243–2245.
12 W. Gao, D. Kagan, O. S. Pak, C. Clawson, S. Campuzano, E. Chuluun-Erdene, E. Shipton, E. E. Fullerton, L. F. Zhang, E. Lauga and J. Wang, *Small*, 2012, **8**, 460–467.
13 T. E. Mallouk and A. Sen, *Sci. Am.*, 2009, 72–77.
14 W. F. Paxton, S. Sundararajan, T. E. Mallouk and A. Sen, *Angew. Chem., Int. Ed.*, 2006, **45**, 5420–5429.
15 W. F. Paxton, K. C. Kistler, C. C. Olmeda, A. Sen, S. K. St Angelo, Y. Y. Cao, T. E. Mallouk, P. E. Lammert and V. H. Crespi, *J. Am. Chem. Soc.*, 2004, **126**, 13424–13431.
16 J. Wang, *ACS Nano*, 2009, **3**, 4–9.
17 S. Sanchez and M. Pumera, *Chem.–Asian J.*, 2009, **4**, 1402–1410.
18 G. A. Ozin, I. Manners, S. Fournier-Bidoz and A. Arsenault, *Adv. Mater.*, 2005, **17**, 3011–3018.
19 Y. Mei, G. Huang, A. A. Solovev, E. B. Ureña, I. Mönch, F. Ding, T. Reindl, R. K. Y. Fu, P. K. Chu and O. G. Schmidt, *Adv. Mater.*, 2008, **20**, 4085–4090.
20 T. Mirkovic, N. S. Zacharia, G. D. Scholes and G. A. Ozin, *Small*, 2010, **6**, 159–167.
21 A. A. Solovev, Y. F. Mei, E. B. Urena, G. S. Huang and O. G. Schmidt, *Small*, 2009, **5**, 1688–1692.
22 M. Garcia, J. Orozco, M. Guix, W. Gao, S. Sattayasamitsathit, A. Escarpa, A. Merkoci and J. Wang, *Nanoscale*, 2013, **5**, 1325–1331.
23 S. Balasubramanian, D. Kagan, C. M. J. Hu, S. Campuzano, M. J. Lobo-Castanon, N. Lim, D. Y. Kang, M. Zimmerman, L. F. Zhang and J. Wang, *Angew. Chem., Int. Ed.*, 2011, **50**, 4161–4164.
24 D. Kagan, S. Campuzano, S. Balasubramanian, F. Kuralay, G. U. Flechsig and J. Wang, *Nano Lett.*, 2011, **11**, 2083–2087.

25 M. Guix, J. Orozco, M. Garcia, W. Gao, S. Sattayasamitsathit, A. Merkoci, A. Escarpa and J. Wang, *ACS Nano*, 2012, **6**, 4445–4451.

26 A. A. Solovev, W. Xi, D. H. Gracias, S. M. Harazim, C. Deneke, S. Sanchez and O. G. Schmidt, *ACS Nano*, 2012, **6**, 1751–1756.

27 W. Xi, A. A. Solovev, A. N. Ananth, D. H. Gracias, S. Sanchez and O. G. Schmidt, *Nanoscale*, 2013, **5**, 1294–1297.

28 K. M. Manesh, M. Cardona, R. Yuan, M. Clark, D. Kagan, S. Balasubramanian and J. Wang, *ACS Nano*, 2010, **4**, 1799–1804.

29 S. Campuzano, D. Kagan, J. Orozco and J. Wang, *Analyst*, 2011, **136**, 4621–4630.

30 J. Wang, *Lab Chip*, 2012, **12**, 1944–1950.

31 S. Sanchez, A. N. Ananth, V. M. Fomin, M. Viehrig and O. G. Schmidt, *J. Am. Chem. Soc.*, 2011, **133**, 14860–14863.

32 G. J. Zhao, M. Viehrig and M. Pumera, *Lab Chip*, 2013, **13**, 1930–1936.

33 A. A. Solovev, S. Sanchez, M. Pumera, Y. F. Mei and O. G. Schmidt, *Adv. Funct. Mater.*, 2010, **20**, 2430–2435.

34 G. J. Zhao, S. Sanchez, O. G. Schmidt and M. Pumera, *Nanoscale*, 2013, **5**, 2909–2914.